

# **Electric-induced reversal of morphogenesis in *Hydra* regeneration**

**Erez Braun<sup>a,\*</sup> and Hillel Ori<sup>b</sup>**

<sup>a</sup>Department of Physics, <sup>b</sup>Faculty of Medicine,

Technion-Israel Institute of Technology, Haifa 32000, Israel.

\*To whom correspondence may be addressed. Email: [erez@physics.technion.ac.il](mailto:erez@physics.technion.ac.il)

**Morphogenesis in whole-body regeneration requires the dynamic interplay of three types of processes: biochemical<sup>1-3</sup>, mechanical<sup>2,4</sup> and electrical<sup>5,6</sup>, which span all scales from the molecular to the entire organism<sup>7</sup>. Despite significant progress in elucidating the role of these processes in morphogenesis, understanding their integration into a robust body-plan remains elusive<sup>8</sup>. Here we employ external electric fields and study their effect on morphogenesis during *Hydra* regeneration. We show the existence of a critical electric field at which the process of morphogenesis halts. Remarkably, above this critical field morphogenesis exhibits reversal dynamics; a fully developed animal flows back into its incipient spheroid morphology, which nevertheless can regenerate again when the amplitude of the external electric field is reduced below criticality. This controlled backward-forward cycle of morphogenesis can be repeated several times. The folding back of morphology is accompanied by the gradual decay of the *Wnt3* activity, a central component of the head organizer in *Hydra*<sup>9,10</sup>, which re-emerges upon renewed regeneration. We further show that electric-induced reversal of morphogenesis is triggered by enhanced electrical activity of the *Hydra* tissue. The external field stimulates an increase in the epithelium spike-like calcium activity, which in turn is demonstrated to follow electrical spike bursts. The existence of a ~1 kHz upper frequency cutoff of the external AC field and the emergence of similar behavior at an elevated external potassium (K<sup>+</sup>) concentration, which is known to depolarize the tissue and increase electrical activity, strengthen the conclusion that enhanced electrical excitability is the underlying mechanism of morphogenesis reversal. The simultaneous morphology reversal and *Wnt3* decay under electrical excitations, demonstrates the tight symbiotic coupling between biochemical, mechanical and electrical processes during morphogenesis. Controlled reversal trajectories open a new vista on morphogenesis and suggest a novel approach to study regeneration as well as potential applications in regenerative medicine.**

Morphogenesis has been shown to involve endogenous electrical processes and be sensitive to perturbations affecting transmembrane voltages<sup>6,11,12</sup>. However, much less is known about the effect of external electrical stimulations on morphogenesis in developmental systems. *Hydra*, a

freshwater animal exhibiting remarkable regeneration capabilities, is an interesting model system for that purpose, due to the excitable nature of its epithelial tissues which are capable of generating and propagating electrical action potentials<sup>13-15</sup>. *Hydra* can regenerate from tissue segments and even cell aggregates<sup>16</sup>. Tissues from all the different initial conditions go through an essential stage in which they form a hollow spheroid made of a bilayer of epithelial cells which eventually regenerates into the body of a mature *Hydra*<sup>17-19</sup>. We place small tissue spheroids formed from tissues fragments excised from adult *Hydra* into ~1.3 mm diameter wells made in an agarose gel placed between a pair of platinum mesh electrodes, 4 mm apart. The tissue spheroids are free to move within the wells and are immersed in a standard *Hydra* medium under continuous flow which ensures constant environmental conditions (Methods). The application of AC fields rather than DC fields which cause extensive hydrolysis, prevents the contamination of the electrodes.

In the absence of external electric fields, *Hydra* regenerate from incipient tissue spheroids into mature animals within 15–55 hrs<sup>18</sup>. The regeneration trajectory is significantly affected by an applied voltage (Fig. 1). The application of an AC electric field with a critical voltage amplitude of ~20–30 Volts at 1 kHz frequency, halts regeneration and the tissue does not develop (Figs. 1a,b; Extended Data Fig. 1). The suspended tissue maintains its regeneration potential as proved by the resumption of morphogenesis upon the reduction of the external voltage below the critical value (Fig. 1b; Extended Data Fig. 1). When the voltage is increased above the critical value after the regeneration process concluded, a fully developed *Hydra* gradually shrinks its tentacles and eventually folds back its mature body-plan into the incipient morphology of a spheroid (Fig. 1c; Extended Data Fig. 2). The reversal of morphogenesis is gradual and can be controlled to some extent by the external voltage. However, different tissues exhibit different critical voltages. The practical difficulty in precisely controlling the morphogenesis trajectory is due to the individual sensitivity of each tissue to the applied voltage and the fact that above the critical value, which cannot be *a-priori* determined, too high external potential can lead to irreversible disintegration of the tissue and loss of its regeneration capability. However, if the voltage increase is gradual and carefully controlled near the critical value, the tissue maintains its integrity as well as its regeneration capacity for repeated cycles of backward-forward morphogenesis (Supplementary Movie 1). This remarkable reversal of morphogenesis is

reproducible and robust as summarized in the cumulative distributions of 15 experiments in Fig. 1d. It shows that below the critical voltage (blue curve, left) regeneration (defined by the emergence of tentacles) emerges for all samples (147) in less than ~55 hrs. At voltages above criticality, however, the probability to observe tentacles in the back-folding samples diminishes within a wide range of time scales, and is practically zero above ~90 hrs. All 77 samples in Fig. 1d (red curve, right) first regenerate into mature animals and then fold back upon the increase of the external voltage.

Renewed morphogenesis upon the reduction of the applied voltage, does not necessarily lead to the same morphology as in the previous cycle, e.g., manifested by different number of tentacles or their shape (Extended Data Fig. 2). The cycles of controlled backward-forward morphogenesis can be repeated a few times. The second cycle of backward folding requires higher voltage to reverse morphogenesis than the first one (see examples in Fig. 4a; Extended Data Fig. 2). This increase in the critical voltage points to an interesting adaptation of the tissue.

We next examine whether reversal morphogenesis has a signature in the underlying biological processes beyond the observed change in morphology. We utilized a transgenic *Hydra* expressing a GFP probe under the control of the *Wnt3* promoter<sup>10, 20</sup>. *Wnt3* is a component of the canonical *Wnt* pathway, which has been shown to be key in patterning the body plan in many organisms and in *Hydra* is an essential component of the head organizer<sup>10, 21</sup>. The *Hydra* head organizer is a well-defined group of cells in which *Wnt3* is maintained continuously active by an autoregulatory transcriptional system<sup>10</sup> and plays an important role in preserving the integrity of the body-plan in face of continuous replacement of tissues in a developmental process that never ceases<sup>22</sup>. The *Wnt3* signal is thus a relevant marker for the underlying biological state of the tissue in morphogenesis. Remarkably, the *Wnt3*-activity fluorescence signal that emerges at the tip of the head (hypostome) in mature *Hydra*<sup>10, 21</sup>, gradually decays after the external voltage is increased beyond criticality, marking the decay of the head organizer activity as the tissue folds back into an incipient spheroid (Fig. 2). The *Wnt3* signal re-emerges upon a second round of regeneration, following switching of the external voltage to zero (Supplementary Movie 2). Overall, we examined 18 samples in 6 different experiments of fully regenerated *Hydra*,

reversing its morphology together with the complete disappearance of the *Wnt3*-activity fluorescence signal (examples in Extended Data Fig. 3).

To gain insight into the mechanism of reversible morphogenesis, we next study the effect of the external field on calcium dynamics. Calcium is an important universal effector across systems and an important mediator between mechanical, electrical and biochemical processes<sup>8</sup>. Towards this end, we constructed a transgenic *Hydra* expressing a fast  $\text{Ca}^{2+}$  fluorescence probe<sup>23</sup> in its epithelial cells (Methods). Tissue fragments excised from these transgenic *Hydra* are placed in the experimental setup after folding into spheroids and time-lapse movies at 1 min resolution are recorded. In the absence of external electric fields, the tissue initially exhibits local excitations of the  $\text{Ca}^{2+}$  signals at different parts of it, which eventually become coordinated into sporadic whole-body coherent spikes (Figs. 3a,b). Elevated external voltage (>15 V, 1 kHz), leads to a significant increase in the  $\text{Ca}^{2+}$  activity manifested in an increased density of the  $\text{Ca}^{2+}$  spikes train riding on an enhanced baseline and a switch into even more enhanced activity above a critical voltage of ~20 V (Fig. 3a, arrow at the lower trace), with prolonged periods showing almost continuous enhanced activity.

Applying an external voltage immediately following the folding of the excised tissue to a spheroid, Fig. 3c (upper trace; Extended Data Fig. 4a) depicts the fluorescence density of the initial spheroid tissue under 15 V (1 kHz). At this voltage, which is somewhat below the critical value, the tissue immediately exhibits a significant level of  $\text{Ca}^{2+}$  activity, which apparently is not enough to halt morphogenesis (see attached images, Fig. 3d; Extended Data Fig. 4a). Increasing the voltage above criticality however, increases the level of  $\text{Ca}^{2+}$  activity (Fig. 3c, middle trace; Extended Data Fig. 4b) causing in turn the folding of the already patterned *Hydra* back into the incipient spheroid (upper image in Fig. 3e; Extended Data Fig. 4b). Finally, switching the voltage to zero reduces  $\text{Ca}^{2+}$  activity (Fig. 3c, bottom trace; Extended Data Fig. 4c) and leads to the recovery of morphogenesis and renewed regeneration of a mature *Hydra* (lower image in Fig. 3e; Extended Data Fig. 4c ), indicating that the tissue maintained its regeneration potential (Supplementary Movie 3). The  $\text{Ca}^{2+}$  activity is quantitatively characterized by the normalized distributions of fluorescence densities in Fig. 3f, summarizing 9 samples overall with more than

10,000 measurement points at 1 min resolution for each curve. It shows enhanced tails with high  $\text{Ca}^{2+}$  activity at elevated external voltages (red) compared to zero voltage (blue).

We next show that the elevated  $\text{Ca}^{2+}$  activity leading to reversal of morphogenesis is a manifestation of enhanced electrical excitability. This is demonstrated along three different experimental lines. First, we demonstrate the existence of a frequency cutoff for the AC electric field, above which the tissue becomes insensitive to the applied field; morphogenesis proceeds normally and no reversal is observed. Fig. 4a shows  $\text{Ca}^{2+}$  traces at two different frequencies of the external field. The initial tissue spheroid first regenerates into a mature *Hydra* at  $V=0$ , showing a typical low level of  $\text{Ca}^{2+}$  activity (Fig. 4a, first trace; Extended Data Fig. 5a).

Increasing the external voltage above the critical value (26.5 V) at 1 kHz, leads to a significant elevation in the level of  $\text{Ca}^{2+}$  activity and folding of the mature *Hydra* back into a spheroid morphology (Fig. 4a, second trace; Extended Data Fig. 5b). Increasing the AC frequency to 3 kHz while maintaining the same amplitude, results in reduced  $\text{Ca}^{2+}$  activity and re-emergence of a regenerated mature *Hydra* (Fig. 4a, third trace; Extended Data Fig. 5c). The frequency sensitivity is summarized in Fig. 4b, showing the normalized distributions of fluorescence density at zero and high voltage at 1 kHz (20-26.5 V) and 3 kHz (26.5 V). The  $\text{Ca}^{2+}$  activity at 3 kHz is very comparable to that at zero voltage, while the activity at 1 kHz is significantly enhanced. Repeating this frequency-switching cycle, Fig. 4a (fourth trace) shows the re-emergence of an elevated  $\text{Ca}^{2+}$  activity and backwards folding of morphogenesis into a spheroid upon switching back to 1 kHz. This second cycle of backward folding however, requires higher critical voltage to reverse morphogenesis than the first one ( $V>30$  V). Finally, switching frequency again to 3 kHz reduces  $\text{Ca}^{2+}$  activity and leads to the emergence of a re-regenerated mature *Hydra* (Fig. 4a, bottom trace). These data demonstrate the existence of a frequency cutoff around 1 kHz, above which the elevated  $\text{Ca}^{2+}$  activity is reduced and morphogenesis is restored from its suspended state. Further experiments demonstrate that at frequencies higher than 1 kHz, the regeneration process is insensitive to the external electric field (Supplementary Movie 4). The ~1 kHz frequency threshold, above which the tissue becomes “transparent” to the applied external voltage, strongly suggests a corresponding characteristics timescale of the order of a few milliseconds, which is consistent with the measured capacitance (RC) time constant of the *Hydra* tissue<sup>24</sup>.

Second, we follow the tissue dynamics under an elevated external potassium ( $K^+$ ) concentration which serves as a standard method to stimulate excitable tissues, as demonstrated also in *Hydra*<sup>25</sup>. Fig. 4c shows that increasing potassium concentration in the medium from 0.1 mM (normal medium; upper trace) to 1 mM (lower trace), indeed leads to elevated  $Ca^{2+}$  activity (see also the normalized distributions in Fig. 4d). Importantly, this is accompanied by folding back of the regenerated *Hydra*. The tissue seems to lose its regeneration capability following the high potassium treatment. Nevertheless, it is clear that elevated potassium excites the system and leads to reversal morphogenesis similar to that observed under an external electric field (Extended Data Fig. 6).

Finally, we directly measure the time-dependent electrical potential by inserting a silver-chloride electrode into a tissue segment embedded in a low-melting 2% agarose gel that damps its motion, while simultaneously recording fluorescence images of the  $Ca^{2+}$  signal under the microscope. Fig. 4e shows that every  $Ca^{2+}$  spike is stimulated by a pre-burst of action potentials<sup>14, 26</sup> (167/174 measured  $Ca^{2+}$  spikes show clear pre-bursts of action potentials leading them; see also Extended data Fig. 7).

These three pieces of evidence: frequency threshold, excitations due to elevated potassium and direct electrical recordings, point to enhanced electrical activity of the *Hydra* tissue as the source of elevated  $Ca^{2+}$  activity and thus to the mechanism triggering reversal morphogenesis. Previous works indeed showed that external electric fields, within the same range used in our experiments, cause enhanced electrical activity, leading for example to enhanced discharge of nematocytes<sup>25</sup>.

While the mechanism leading from enhanced  $Ca^{2+}$  activity to reversal of morphogenesis requires further research, the observed phenomenon whereby this reversal process is driven by electrical excitations has already at this stage some important implications. First, morphogenesis is usually considered a hierarchical forward-driven process, in which each stage switches-on the next one till the completion of a body plan<sup>27</sup>. It was shown before that under metabolic stress *Hydra* can lose its tentacles and change its body morphology in a reversible way, but this phenomenon was not further investigated<sup>28</sup>. The observation that an external physical manipulation in the form of an electric field, by triggering enhanced electrical excitations of the tissue, can halt morphogenesis and even reverse it in a controlled way without destroying the regeneration

potential of the tissue, paints a picture of morphogenesis in which electrical processes play an instructive role to a level that could direct developmental trajectories that do not obey this hierarchy<sup>5</sup>. Second, it shows that the electrical processes are tightly integrated with the underlying mechanical (e.g., tissue folding)<sup>8</sup> and biochemical (e.g., *Wnt3* expression) ones. In particular, the decay of the head organizer during reversal of morphogenesis demonstrates that the changes in the tissue encompass more than mere morphology, and also involve significant rearrangements in the underlying biological processes. How deep these biological transformations are, e.g. in reprogramming differentiated cells into stem cells, remains an exciting question for future studies. The ability to stimulate reversal of morphogenesis by an external electric field opens up new ways to further study the symbiotic dynamics of these different processes in morphogenesis. In particular, the ability to halt morphogenesis at different time points and reverse its dynamic trajectory enables us to identify the types of information stored in the developing tissues, the reservoirs of ions and biomolecules and structural memories<sup>18</sup> instilled in the tissue and playing a role in the regeneration process. Furthermore, the ability to block regeneration in a controllable fashion can shed light on the origin of a tissue's regeneration potential and reveal the reasons some tissues can readily regenerate while others cannot do so.

Third, controlled reversal morphogenesis opens the possibility for a new approach in the study of developmental systems, in general<sup>29, 30</sup>: One would like to study the potential of a given system to realize different developmental trajectories, beyond the canalized one<sup>8</sup>. Currently, this can be done only by studying an ensemble of different systems. Halting, reversing and re-initiating a developmental process of a given system at different time points, open up a possibility for studying the developmental potential rather than an instantiation of it.

## **Acknowledgements**

We thank Kinneret Keren for helpful discussions and comments on the manuscript. We thank Shimon Marom and Naama Brenner for comments on the manuscript. We thank our lab members: Anton Livshits, Lital Shani-Zerbib, Yonit Maroudas-Sacks and Liora Garion for technical help. Special thanks to Gdalyahu Ben-Yoseph for superb technical help in designing



and constructing the experimental setup and in providing the infrastructure enabling the experiments.

We thank Prof. Thomas Bosch and Dr. Alexander Klimovich for their help in generating the  $\text{Ca}^{2+}$  strain; Prof. Bert Hobmayer for generously providing the transgenic *Hydra* expressing lifeact;

Prof. Brigitte Galliot for generously providing the *Wnt3* strain that was first constructed in Prof. Thomas Holstein lab.

E.B. acknowledged support by the Israel Science Foundation, Grant # 228/17.

## Materials and Methods

### *Hydra strains, culture and sample preparation*

Experiments are carried out with three transgenic strains of *Hydra Vulgaris* (AEP): A HyWnt3:GFP-HyAct:dsRED transgenic strain (a gift from B. Galliot University of Geneva<sup>20</sup> utilizing the hoTG-HyWnt3FL-EGFP-HyAct:dsRED plasmid from T. Holstein, Heidelberg<sup>10</sup>); A transgenic line with a GCaMP6s probe reporting  $\text{Ca}^{2+}$  activity we generated in the Kiel center using a modified version of the pHyVec1 plasmid (Addgene catalog no. 34789) which replaces the GFP sequence with a GCaMP6s sequence that was codon-optimized for *Hydra*<sup>23</sup>. The embryos were grown and propagated for a few weeks. We selected *Hydra* expressing GCaMP6s in their epithelium cells and propagate them until a stable signal covering the entire animal emerges throughout the population. A third transgenic line expressing lifeact-GFP in the ectoderm (generously provided by Prof. Bert Hobmayer, University of Innsbruck, Austria)<sup>18</sup>, is also used in some experiments, allowing to verify the folding-back of the *Hydra* into a spheroid by imaging the actin fibers. The reversal of morphogenesis phenomenon is found to be similar for all strains. Animals are cultivated in *Hydra* culture medium (1mM  $\text{NaHCO}_3$ , 1mM  $\text{CaCl}_2$ , 0.1mM  $\text{MgCl}_2$ , 0.1mM KCl, 1mM Tris-HCl pH 7.7) at 18°C. The animals are fed every other day with live *Artemia nauplii* and washed after ~4 hours. Experiments are initiated ~24 hours after feeding.

Tissue segments are excised from the middle of a mature *Hydra* using a scalpel equipped with a #15 blade. To obtain fragments, a ring is cut into ~4 parts by additional longitudinal cuts. Fragments are incubated in a dish for ~3 hrs to allow their folding into spheroids prior to transferring them into the experimental sample holder. Regeneration is defined as the appearance of tentacles, and the regeneration time is defined as the time interval between excision and the appearance of the first tentacle.

### *Sample holder*

Spheroid tissues are placed within wells of ~1.3 mm radius made in a strip of 2% agarose gel (Sigma) to keep the regenerating *Hydra* in place during time lapse imaging. The tissue spheroid typically of a few hundred  $\mu\text{m}$  is free to move within the well. The agarose strip containing 12-13 wells, is fixed on a transparent plexiglass bar of 1 mm height, anchored on a Teflon holder within a 55 mm Petri dish. Two platinum mesh electrodes (Platinum gauze 52 mesh, 0.1 mm dia. Wire; Alfa Aesar) are stretched and fixed by 2% agarose gel from the two sides of the plexiglass bar at a distance of 4 mm, leaving two channels for fluid flow between the electrodes and the samples. The mesh electrodes cover the entire length of the sample holder and their height ensures full coverage of the samples. A peristaltic pump (IPC, Ismatec) flows the medium continuously from an external reservoir (replaced at least once every 24 hrs) at a rate of 170 ml/hr into each of the channels between the electrodes and the samples. The medium covers the entire preparation and the volume in the bath is kept fixed throughout the experiments by pumping medium out from 3 holes which determine the height of the fluid. The continuous medium flow ensures stable environmental conditions and the fixed volume of medium in the bath ensures constant conductivity between the electrodes. All the experiments

are done at room temperature.

### ***AC generators***

An alternating current (AC) generator (PM5138A, Fluke; or a waveform generator 33621A, Agilent connected to a voltage amplifier A-303, A.A. Lab Systems for voltages above 40 V) is used to set the voltage between the electrodes. The generator is connected directly to one of the electrodes and via a current multimeter (34401A, HP) to the second one, allowing to monitor the current in the system throughout the experiment. The measured current is around 4 mA for applied 10 V and the conductivity is found to be linear with the increase of applied voltage throughout the experiment. The connection to the platinum electrodes is made by sintering 0.4 mm wide platinum wires (Alfa Aesar) to the mesh electrodes, allowing contacts to the external devices with only Pt touching the medium.

### ***Microscopy***

Time lapse bright-field and fluorescence images are taken by a Zeiss Axio-observer microscope (Zeiss) with a 5× air objective (NA=0.25) with a 1.6× optovar and acquired on a CCD camera (Zyla 5.5 sCMOS, Andor). The sample holder is placed on a movable stage (Marzhauser) and the entire microscopy system is operated by Micromanager, recording images at 1 min resolution.

### ***Electrophysiology***

Tissue fragments before folding or tissue spheroids after folding, are immersed in 2% low-gelling agarose (Sigma) covered with a standard medium, placed within a 90 mm petri dish. The measurements are done under a fluorescence microscope (Zeiss Observer), allowing simultaneous fluorescence and electrical measurements. Microelectrodes are fabricated by AgCl coated silver wires, threaded in glass capillaries (1.5mm OD and 0.86mm ID, A-M systems). Capillaries are pulled, broken at the extreme tip, and filled with a standard medium solution. A reference electrode made of a thick AgCl coated silver wire is immersed in the dish. The microelectrode is placed on a manipulator and allowed to penetrate the tissue until a stable resting potential is measured. Voltage is measured using AxoPatch 200B amplifier (Axon Instruments) and measurements are inspected by an oscilloscope, as well as digitally acquired at 1000Hz frequency by NI PCI-6259 acquisition card (National Instruments). Time lapse imaging is done at 1 min resolution in bright field and fluorescence channels allowing to image the tissue and record the  $\text{Ca}^{2+}$  activity.

To extract the recorded spike train, the voltage trace is smoothed (0.1 sec window) and the smoothed trace is subtracted from the original voltage trace. The filtered trace is magnified to emphasize the spikes. The  $\text{Ca}^{2+}$  activity recorded by the time-lapse fluorescence signal is extracted from each frame within a circle smaller than the tissue fragment to avoid edge

effects. The  $\text{Ca}^{2+}$  signal is manually adjusted to the electrical recording by monitoring the precise starting point of the time-lapse measurement.

## Figures:

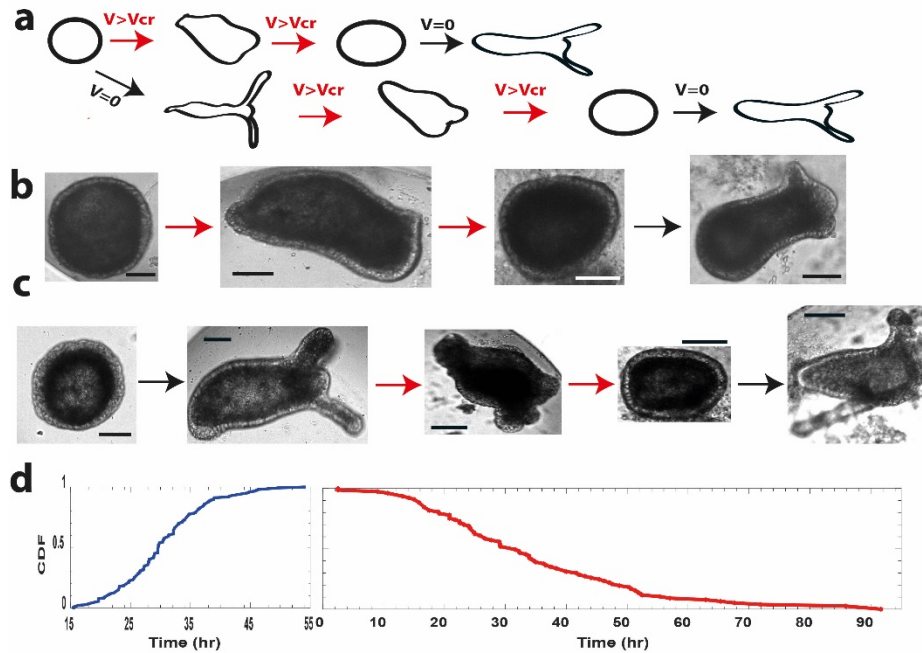


**Fig. 1: Halt and reversal of morphogenesis under an external electric field.** (a) Possible trajectories for an incipient spheroid tissue under a field. Applying voltages above the critical value at the onset, the incipient spheroid does not develop beyond some initial attempts to deform its shape and it is stabilized eventually in a spheroid-like morphology as long as the voltage remains high. Reducing the voltage below criticality leads to regeneration of the suspended tissue into a mature *Hydra* (top row). In the absence of an external field, the incipient spheroid regenerates into a mature *Hydra*. Applying an external voltage above criticality, leads to reversal of morphogenesis into the incipient spheroid morphology which nevertheless maintains its regeneration capability upon the reduction of voltage below the critical value (bottom row).

(b) A series of images depicting the trajectory scheme in (a) top row: Time (hrs from excising the tissue) and voltages (Volts) for the images (from left): 5.5, 0; 42, 18; 68, 25.5; 97, 0. The voltage is switched off at 71 hrs. Bars 100  $\mu\text{m}$  scale.

(c) A series of images depicting the trajectory scheme in (a) bottom row: Time (hrs from excising the tissue) and voltages (Volts) for the images (from left): 2, 0; 53, 0; 80, 25; 108, 31; 136, 0. The voltage is switched off at 108 hrs. Bars 100  $\mu\text{m}$  scale.

(d) Cumulative statistics for regeneration and reversal of morphogenesis. Overall, samples from 15 experiments were analyzed for each curve. (left) Regeneration cumulative statistics for 147 samples exhibiting their first regeneration in the absence of an external voltage or a voltage below the critical value. Time is measured from the point of excision of the tissue fragment and regeneration is identified as the emergence of tentacles. All samples regenerated between 15-55 hrs, in agreement with previous

results<sup>18</sup>. (right) Cumulative statistics for reversal of morphogenesis, the folding back of fully regenerated *Hydra* into the incipient spheroid morphology, for 77 samples. All the samples first regenerated into a mature *Hydra*. Folding time is estimated from the point at which the voltage was first set above 15 V, the minimal voltage observed to affect morphology (e.g., shortening of the tentacles). Due to tissue individual sensitivity to the applied voltage and differences in the critical voltage between samples (which cannot be *a-priory* determined), different points of fold-back occur at different voltages (ranging from 18 V to 37 V). Thus, the folding time (10-90 hrs) is a rough estimate which nevertheless demonstrates the reproducibility and robustness of the reversal of morphogenesis phenomenon.

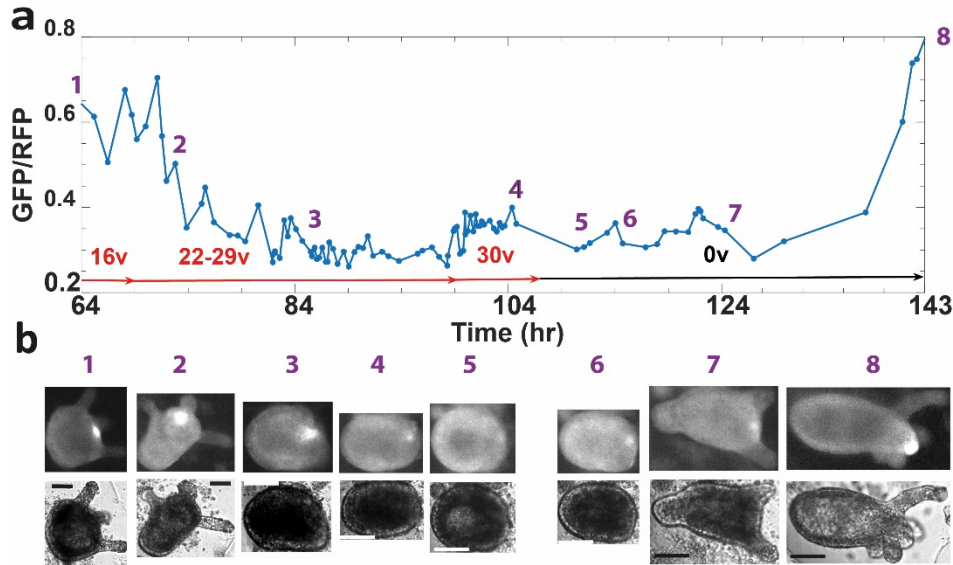


**Fig. 2: The decay of *Wnt3* activity upon reversal of morphogenesis.** Transgenic *Hydra* expressing a GFP probe under the control of the *Wnt3* promoter<sup>10, 20</sup> is imaged under a time-lapse fluorescence microscope at 1 min resolution. This transgenic *Hydra* is also expressing dsRED (RFP) under the control of the ubiquitous *Hydra* actin promoter, which serves as a fluorescence reference (Extended data Fig. 3). (a) The *Wnt3* activity at different time points (measured from the excision time of the tissue fragment) is estimated from the fluorescence ratio of GFP/RFP in a small region around the center of the GFP signal. The tissue is first regenerated into a mature *Hydra* in the absence of an external field, expressing a clear GFP signal at the head organizer in the hypostome. Application of an external field above the critical voltage, leads to reversal of morphogenesis and the decay of the *Wnt3* signal (1-5). Resumption of regeneration leading to a mature *Hydra* and the reemergence of the *Wnt3* signal after the voltage is switched off (6-8). The curve measures the trajectory of the *Wnt3*-activity decay, as the voltage is increased (Voltage values marked in red), and its recovery upon the renewal of regeneration. (b) Fluorescence images of the GFP channel (upper row) and the corresponding bright-field images (lower row) at time points marked in (a). Bars 100  $\mu$ m scale.

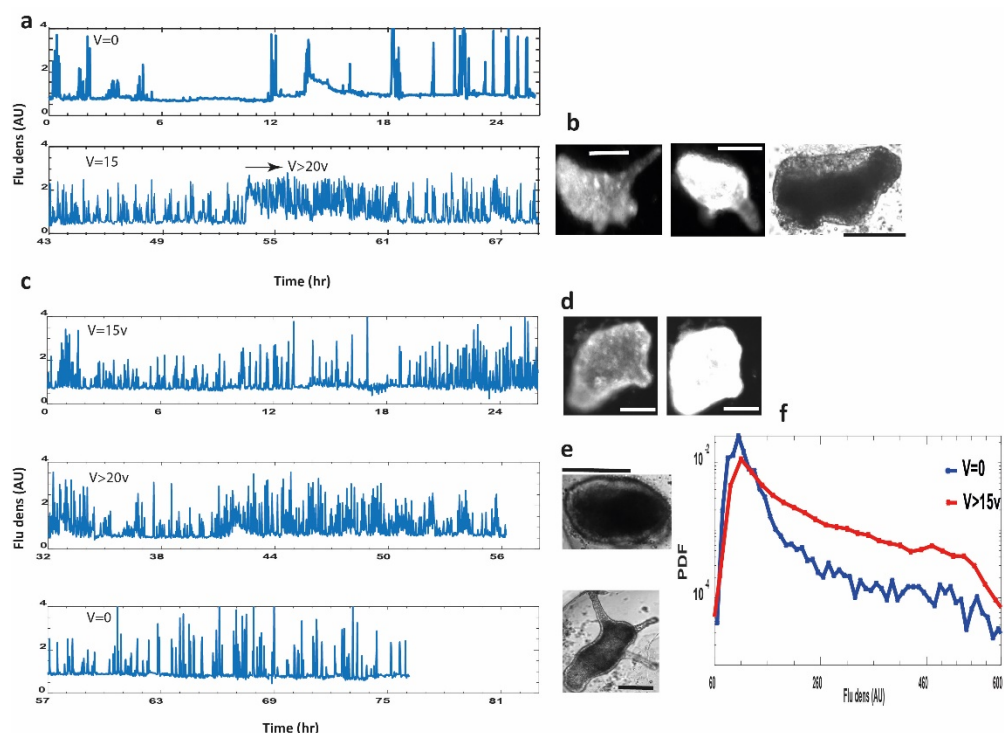


**Fig. 3: Calcium dynamics.** A transgenic *Hydra* expressing the fast Ca<sup>2+</sup> fluorescence probe<sup>23</sup> in its epithelial cells is utilized to measure calcium activity by fluorescence time-lapse at 1 min resolution. (a) Ca<sup>2+</sup> dynamics as measured by the fluorescence density (fluorescence signal per unit area) at V=0 (upper trace) and at high external voltage (lower trace). The measurement starts 3 hrs after the tissue excision. The lower trace starts at 15 V, which is below the critical value, and the voltage is increased to higher values (25 V) from the point marked by the arrow. The traces show the fluorescence density divided by the mean over the entire trace. (b) Fluorescence images of the sample (at the end of the trace), demonstrating the contrast between the baseline and high activity (two left images: 69 hrs from excision, 25 V). The right BF image shows that the tissue folded at later times (79 hrs from excision, 25 V). (c) Ca<sup>2+</sup> activity (as in (a)) of a tissue under a voltage at the onset of the measurement. The measurement starts 3 hrs after the tissue excision at 15 V which is below the critical value (upper trace). The voltage is then increased to higher values (24 V) in the middle trace and then switched off at the lower trace. (d) Fluorescence images of the tissue at the end of the upper trace, showing low and high Ca<sup>2+</sup> activity (29 hrs from excision, 15 V). Note the tentacles indicating that the tissue regenerated. (e) Bright field images showing reversal of the regenerated *Hydra* into a spheroid morphology for the end of the middle trace, and resumption of regeneration leading to a mature *Hydra* at the end of the lower trace (top image: 63 hrs from excision, 24 V; lower image: 77 hrs from excision, 0 V). (f) Normalized distributions of fluorescence densities at V=0 (blue) and high voltage (>15 V; red). Each curve summarizes the measurements of 9 samples overall with more than 10,000 measurement points. Note the logarithmic scale. The distributions show enhanced Ca<sup>2+</sup> activity at elevated external voltages (V>15 V) compared to zero voltage.



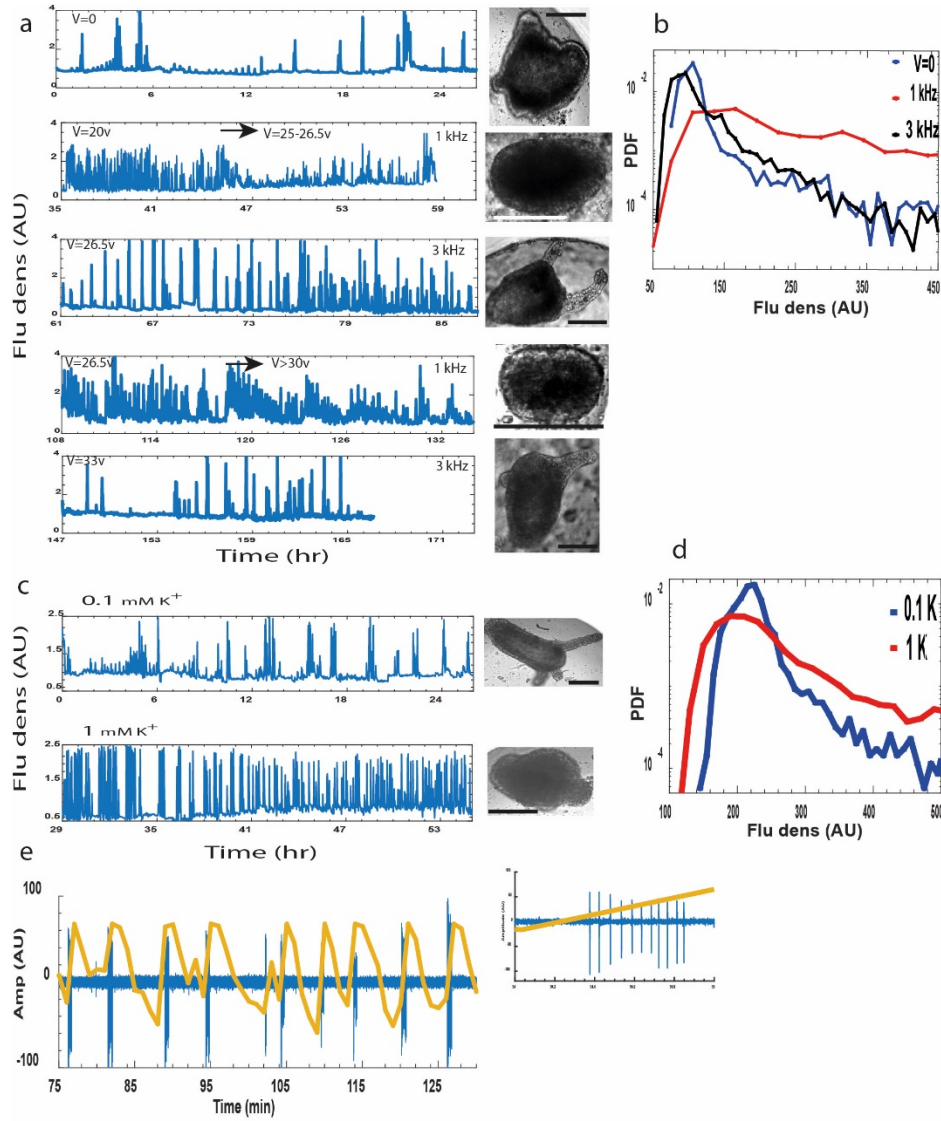


**Fig. 4: Enhanced electrical excitability of the tissue triggering reversal of morphogenesis.** (a)  $\text{Ca}^{2+}$  activity measured by the fluorescence density (as in Fig. 3), for two different frequencies of the external AC electric field. The measurement starts 3 hrs after the tissue excision at  $V=0$  (first trace) and continues at high voltage (20-26.5 V) at 1 kHz (second trace), showing enhanced  $\text{Ca}^{2+}$  activity. The attached images (at the end point of each corresponding trace) show that the tissue fully regenerated for  $V=0$  and then folded back into a spheroid morphology at high voltage. Switching the frequency of the external field to 3 kHz, while maintaining the voltage amplitude at 26.5 V, shows reduction in  $\text{Ca}^{2+}$  activity (third trace) and resumption of a fully regenerated *Hydra* (attached image). The frequency sensitivity is summarized in the normalized distributions of fluorescence density in (b), comparing zero voltage statistics (blue) with that of high voltage at 1 kHz (red) and 3 kHz (black). Each curve summarizes measurements over two samples, with 2800-4500 measured points at 1 min resolution. Note the logarithmic scale. The cycle of frequency switching is then repeated by setting the frequency again to 1 kHz at the same voltage (26.5 V; fourth trace) which shows an enhanced  $\text{Ca}^{2+}$  activity. The applied field however, is now below the critical value. Increasing the voltage further (33 V), leads to reversal of morphogenesis and folding of the tissue into a spheroid morphology (attached image). Finally, a second frequency switch to 3 kHz (fifth trace) shows again reduction in  $\text{Ca}^{2+}$  activity and resumptions of regeneration. Note that the critical

voltage is higher in this second cycle of frequency switch compared to the first one, due to adaptation of the tissue.

(c)  $\text{Ca}^{2+}$  activity measured by fluorescence density (as in a) for two concentrations of potassium ( $\text{K}^+$ ) in the medium; 0.1 mM (normal Hydra medium; upper trace) and 1 mM (lower trace). The measurement starts 3 hrs after the tissue excision. The fluorescence density shows enhanced  $\text{Ca}^{2+}$  activity for the higher potassium concentration. The attached images (at the end point of the corresponding trace) show that the tissue fully regenerated for the upper trace and folded back into a spheroid at the lower trace. (d) Fluorescence density distributions for the two potassium concentrations showing an extended elevated tail for 1 mM (red) compared to 0.1 mM (blue). Note the logarithmic scale.

(e) Direct measurement of the time-dependent electrical potential. A silver-chloride electrode was inserted into a tissue segment embedded in a low-melting 2% agarose gel, while simultaneously recording fluorescence images. Each  $\text{Ca}^{2+}$  spike (yellow) is stimulated by a pre-burst of action potentials (blue). Note the time scale in minutes. See Methods for the extraction of the electrical spikes. The inset is a zoom over one of the  $\text{Ca}^{2+}$  spike events, showing clearly the burst of electrical spikes. Overall we measured 107  $\text{Ca}^{2+}$  spikes in tissue fragments with only 5 among them with no clear burst of electrical spikes (see Extended Data Fig. 7b for a measurement of a spheroid tissue).

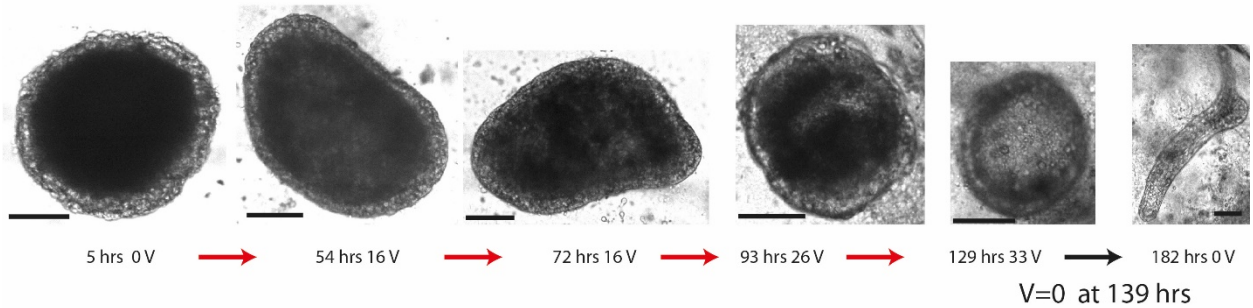
## References:

1. Green, J.B.A. & Sharpe, J. Positional information and reaction-diffusion: two big ideas in developmental biology combine. *Development* **142**, 1203-1211 (2015).
2. Miller, C.J. & Davidson, L.A. The interplay between cell signalling and mechanics in developmental processes. *Nature Rev. Genetics* **14**, 733-744 (2013).
3. Lawrence, P.A. Morphogens: how big is the big picture? *Nature Cell Biology* **3**, E151-E154 (2001).
4. Mammoto, T., Mammoto, A. & Ingber, D.E. Mechanobiology and Developmental Control. *Annual Review of Cell and Developmental Biology* **29**, 27-61 (2013).
5. Levin, M. & Martyniuk, C.J. The bioelectric code: An ancient computational medium for dynamic control of growth and form. *Biosystems* (2017).
6. Levin, M., Pezzulo, G. & Finkelstein, J.M. Endogenous bioelectric signaling networks: Exploiting voltage gradients for control of growth and form. *Annual Review of Biomedical Engineering* **19**, 353-387 (2017).
7. Müller, G.B. & Newman, S.A. in *Vienna Series in Theoretical Biology* (MIT Press, Cambridge, 2003).
8. Braun, E. & Keren, K. Hydra Regeneration: Closing the Loop with Mechanical Processes in Morphogenesis. *BioEssays* **40**, 1700204 (2018).
9. Bode, H.R. Axial Patterning in Hydra. *Cold Spring Harbor Perspectives in Biology* **a000463**, 1 (2009).
10. Nakamura, Y., Tsiairis, C.D., Ozbek, S. & Holstein, T.W. Autoregulatory and repressive inputs localize Hydra Wnt3 to the head organizer. *PNAS* **108**, 9137-9142 (2011).
11. McLaughlin, K.A. & Levin, M. Bioelectric signaling in regeneration: Mechanisms of ionic controls of growth and form. *Developmental biology* **433**, 177-189 (2018).
12. Levin, M. & Martyniuk, C.J. The bioelectric code: An ancient computational medium for dynamic control of growth and form *Biosystems* **164**, 76-93 (2018).
13. Campbell, R.D., Josephson, R.K., Schwab, W.E. & Rushforth, N.B. Excitability of nerve-free hydra. *Nature* **262**, 388-390 (1976).
14. Josephson, R.K. & Macklin, M. Transepithelial Potentials in Hydra. *Science* **156**, 1629-1631 (1967).
15. Kass-Simon, G. & Diesl, V.K. Spontaneous and evoked potentials from dissociated epithelial cells of Hydra. *Nature* **265**, 75-77 (1977).
16. Gierer, A. et al. Regeneration of hydra from reaggregated cells. *Nature/New Biology*, 98-101 (1972).
17. Fütterer, C., Colombo, C., Julicher, F. & Ott, A. Morphogenetic oscillations during symmetry breaking of regenerating Hydra vulgaris cells. *EPL* **64**, 137 (2003).
18. Livshits, A., Shani-Zerbib, L., Maroudas-Sacks, Y., Braun, E. & Keren, K. Structural inheritance of the actin cytoskeletal organization determines the body axis in regenerating hydra. *Cell Reports* **18**, 1410-1421 (2017).
19. Kucken, M., Soriano, J., Pullarkat, P.A., Ott, A. & Nicola, E.M. An osmoregulatory basis for shape oscillations in regenerating Hydra. *Biophys J* **95**, 978-985 (2008).
20. Vogg, M.C. et al. An evolutionarily-conserved Wnt3/ $\beta$ -catenin/Sp5 feedback loop restricts head organizer activity in Hydra. *Nature Communications* **10**, 312 (2019).
21. Hobmayer, B. et al. WNT signalling molecules act in axis formation in the diploblastic metazoan Hydra. *NATURE* **407**, 186-189 (2000).
22. Bode, H.R. The head organizer in Hydra. *Int. J. Dev. Biol.* **56**, 473-478 (2012).

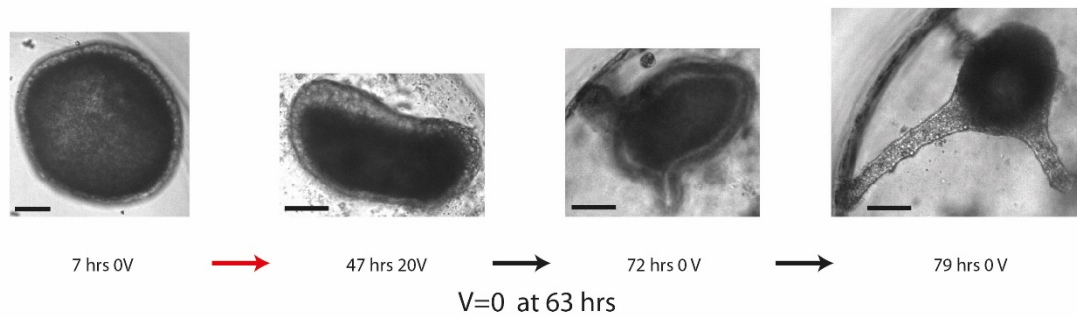
23. Dupre, C. & Yuste, R. Non-overlapping neural networks in *Hydra vulgaris*. *Current Biology* **27**, 1-13 (2017).
24. Josephson, R.K. & Macklin, M. Electrical Properties of the Body Wall of *Hydra*. *The Journal of General Physiology* **53**, 638-665 (1969).
25. Gitter, A.H., Oliver, D. & Thurm, U. Calcium- and voltage-dependence of nematocyst discharge in *Hydra vulgaris*. *Journal of Comparative Physiology A* **175**, 115-122 (1994).
26. Itayama, T. & Sawada, Y. Development of electrical activity in regenerating aggregates of hydra cells. *Journal of Experimental Zoology* **273**, 519-526 (1995).
27. Gilbert, S.F. *Developmental Biology* (Sinauer Associates, Inc., 2013).
28. Newman, S.A. Reversible Abolition of Normal Morphology in *Hydra*. *Nature New Biology* **244**, 126 (1973).
29. Vygotsky, L.S. in *Mind in Society; the Development of Higher Psychological Processes* (eds. Cole, M., John-Steiner, V., Scibner, S. & Souberman, E.) 58-79 (Harvard University Press, Cambridge Mass, 1978).
30. Marom, S. *Science, Psychoanalysis, and the Brain: space for dialogue* (Cambridge University Press, New York, 2015).

## Extended Data figures:

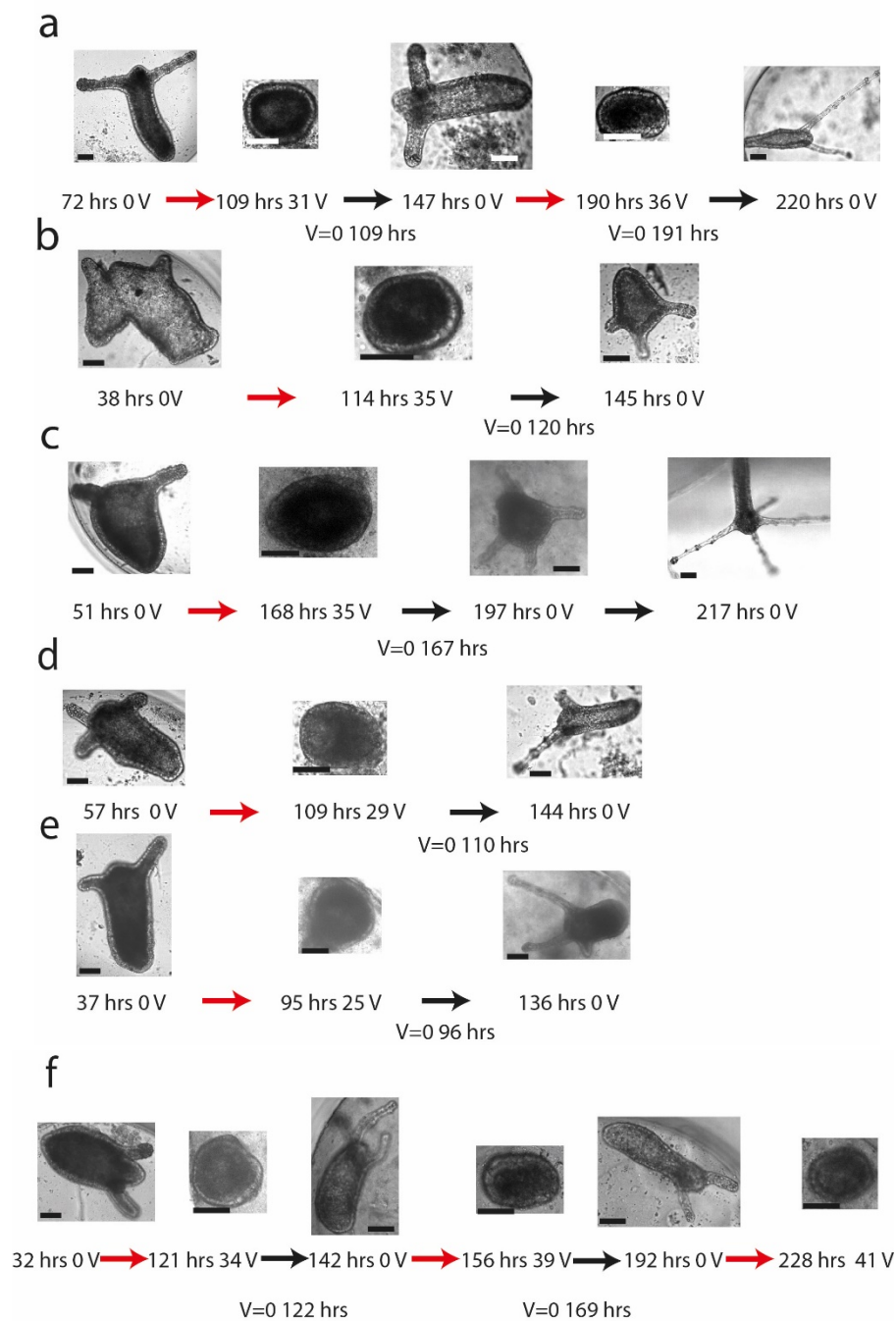
a



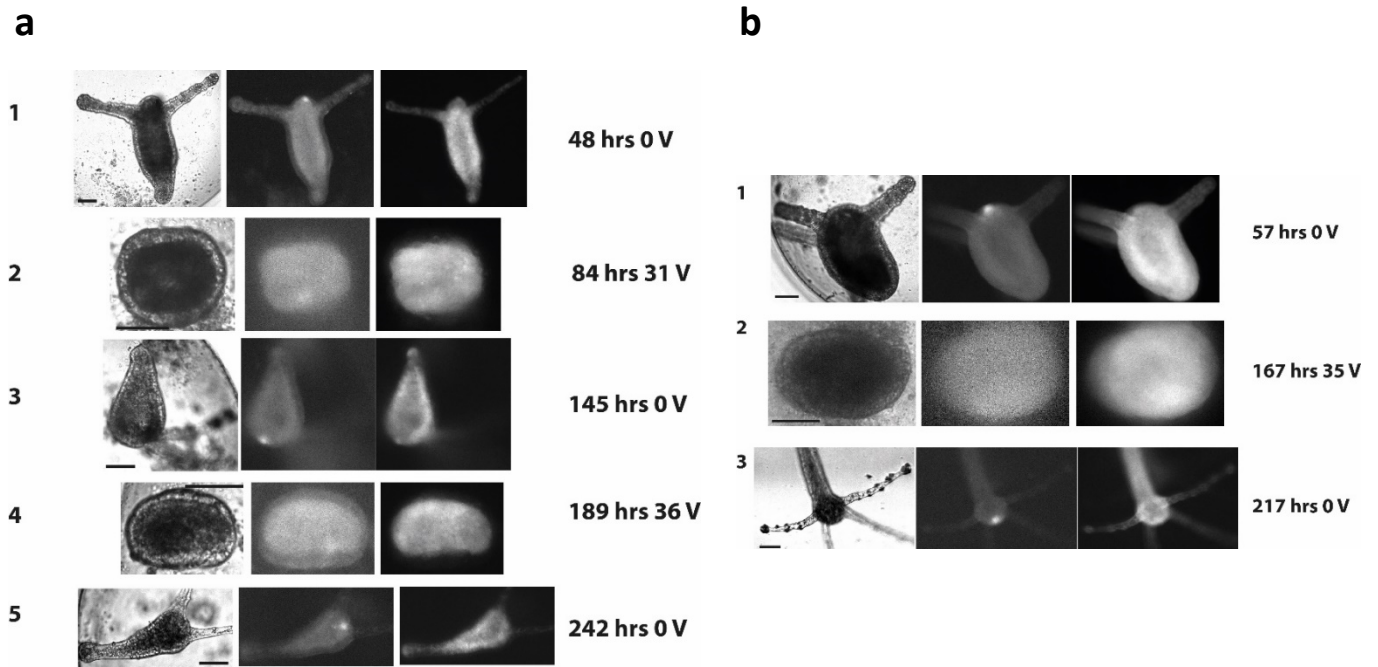
b



**Extended Data Fig. 1: Examples of halted regeneration by an external electric field.** A series of images from two experiments (a, b) depicting the trajectory scheme in Fig. 1a top row of the main text. Time (hrs from excising the tissue) and voltages (Volts) are indicated for each image. The tissues do not develop under the electric field above its critical value (specific for each tissue; 1 kHz) until time points extending the maximal regeneration time observed in our experiments (~55 hrs) and they readily regenerate into a mature *Hydra* upon switching the voltage to zero at the indicated time. Bars 100  $\mu$ m scale.



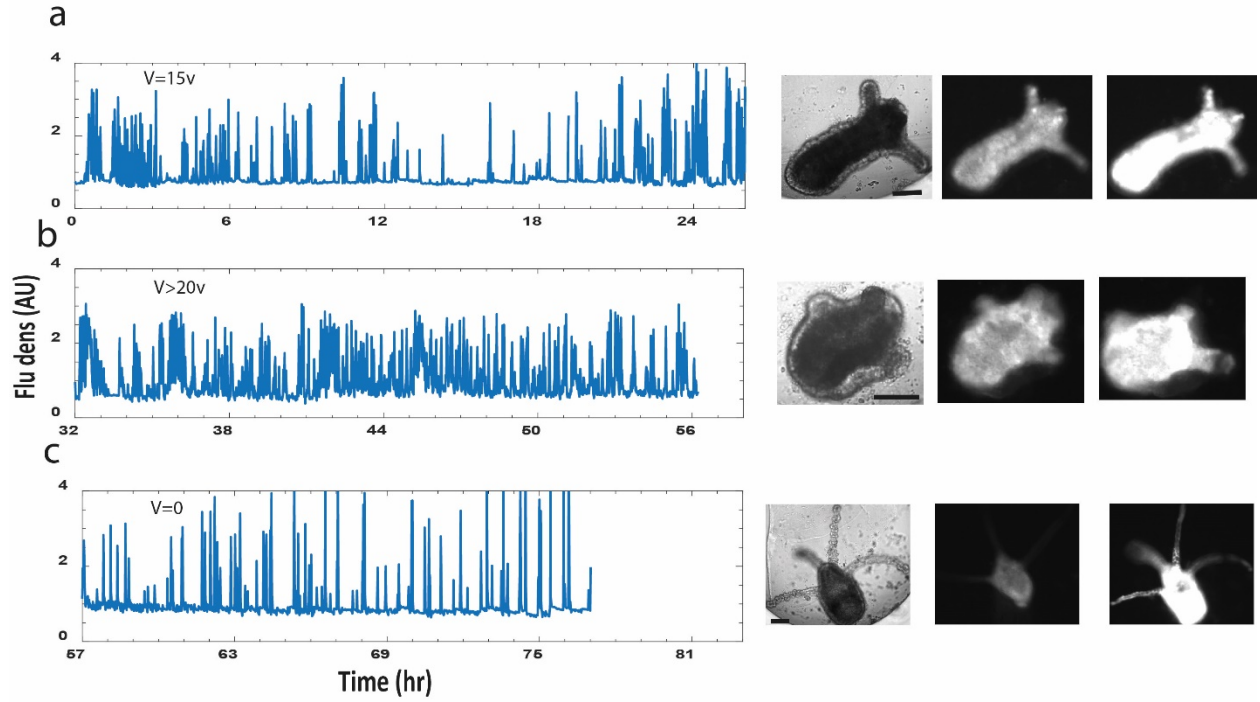
**Extended Data Fig. 2: Examples of reversal of morphogenesis under an external electric field and the emergence of new morphologies upon renewal of regeneration.** A series of images depicting the trajectory scheme in Fig. 1a bottom row of the main text. Each row of images (a-f) is a separate experiment. Time (hrs from excising the tissue) and voltages (Volts) are depicted below the images (external AC field at 1 kHz). In all the experiments presented here, the spheroid tissue first regenerates into a mature Hydra and then folds back into a spheroid upon the increase of the externally applied voltage above the critical value (specific for each tissue). The reversed tissue regenerates again upon the reduction of the external voltage to zero at the indicated time. Note that the emerged renewal morphology is in some of the cases not similar to the initial morphology. The images in (a,f) demonstrate that this backward-forward cycle of morphogenesis can be repeated for the same tissue. Bars 100  $\mu$ m scale.



**Extended Data Fig. 3: Examples of the *Wnt3* activity decay upon reversal of morphogenesis.**

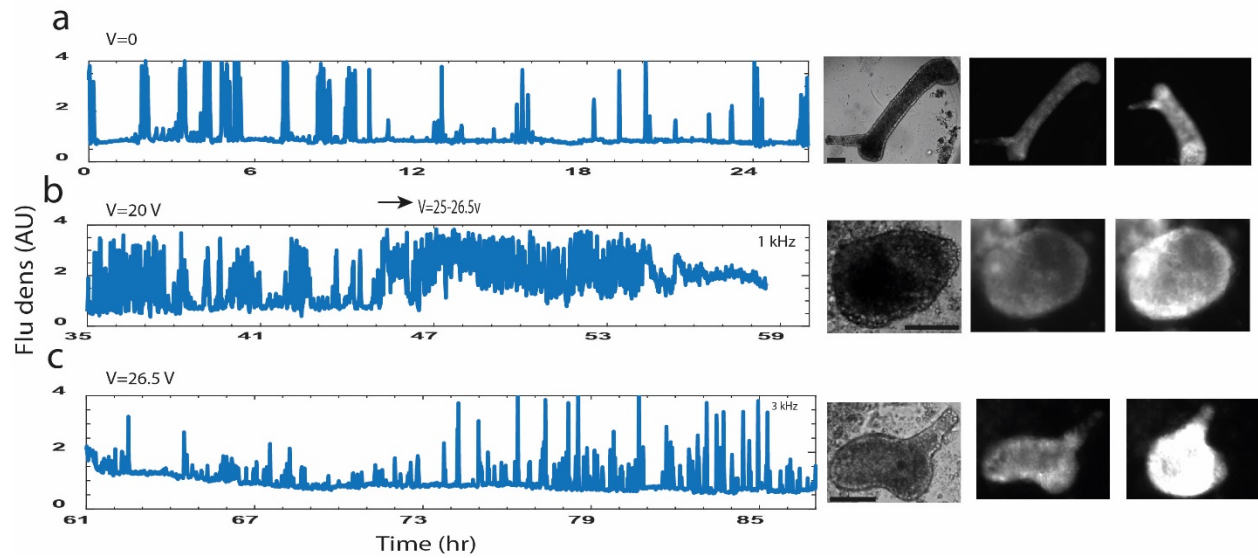
Transgenic *Hydra* expressing a GFP probe under the control of the *Wnt3* promoter<sup>10, 20</sup> is imaged under a fluorescence microscope with time-lapse images taken every 1 min (as in Fig. 2 in the main text). This transgenic *Hydra* is also expressing dsRED (RFP) under the control of the ubiquitous actin promoter, serving as a fluorescence reference. Two experiments (a, b) are shown as a sequence of 3 images (from left: bright field, GFP, RFP) over time. The running time (hrs from the point of tissue excision) and the applied external voltage are depicted to the right of the images. A clear fluorescence signal of GFP under the *Wnt3* promoter at the head of a transgenic *Hydra* emerges after the initial spheroid tissue regenerates (1) and decays upon the reversal of morphogenesis in (2). The *Wnt3*-activated fluorescence reemerges upon renewal regeneration after the voltage is switched off in (3). The experiment in (a) demonstrates a second cycle of reversal morphogenesis (4) and renewal of regeneration leading to re-emergence of the *Wnt3*-activity fluorescence signal. Bars 100  $\mu$ m scale.



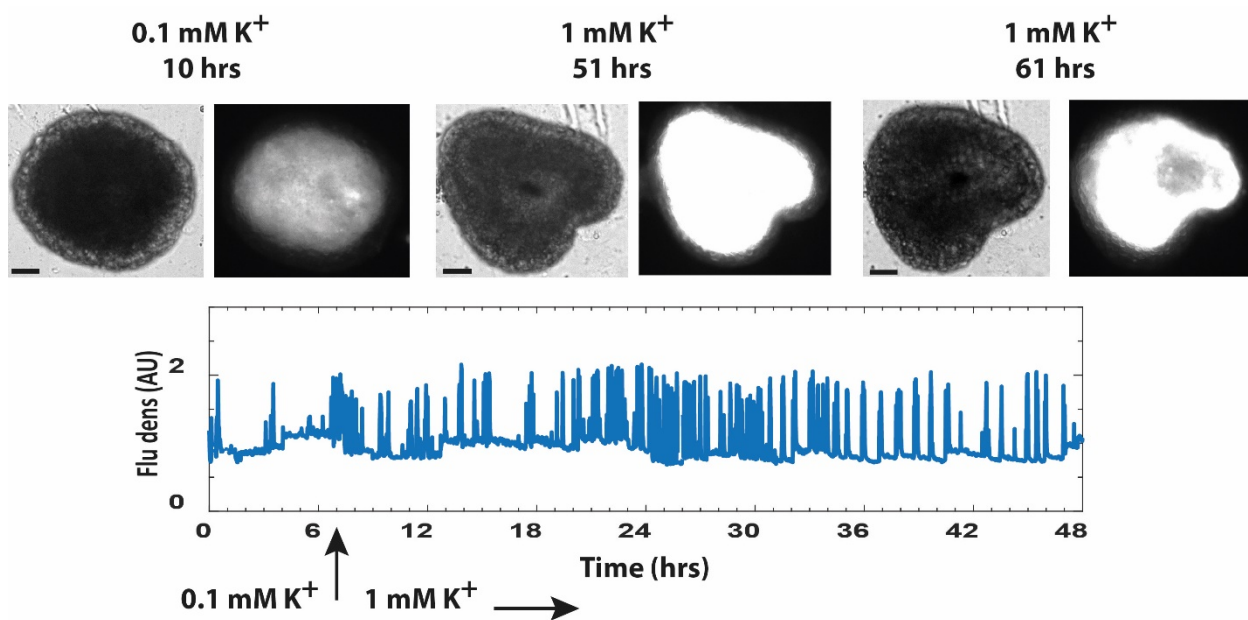


**Extended Data Fig. 4: Calcium dynamics.** (a)  $\text{Ca}^{2+}$  dynamics as measured by the fluorescence density (fluorescence signal per unit area) as in Fig. 3c in the main text. The measurement starts 3 hrs after the tissue excision at 15 V which is below the critical value (a). The voltage is then increased to higher values (24 V) in (b) and then switched off in (c). The images on the right show microscopy images of the sample at the end point of each trace (from left: bright field, low and high  $\text{Ca}^{2+}$  activity depicted by the fluorescence images). Bars 100  $\mu\text{m}$  scale.

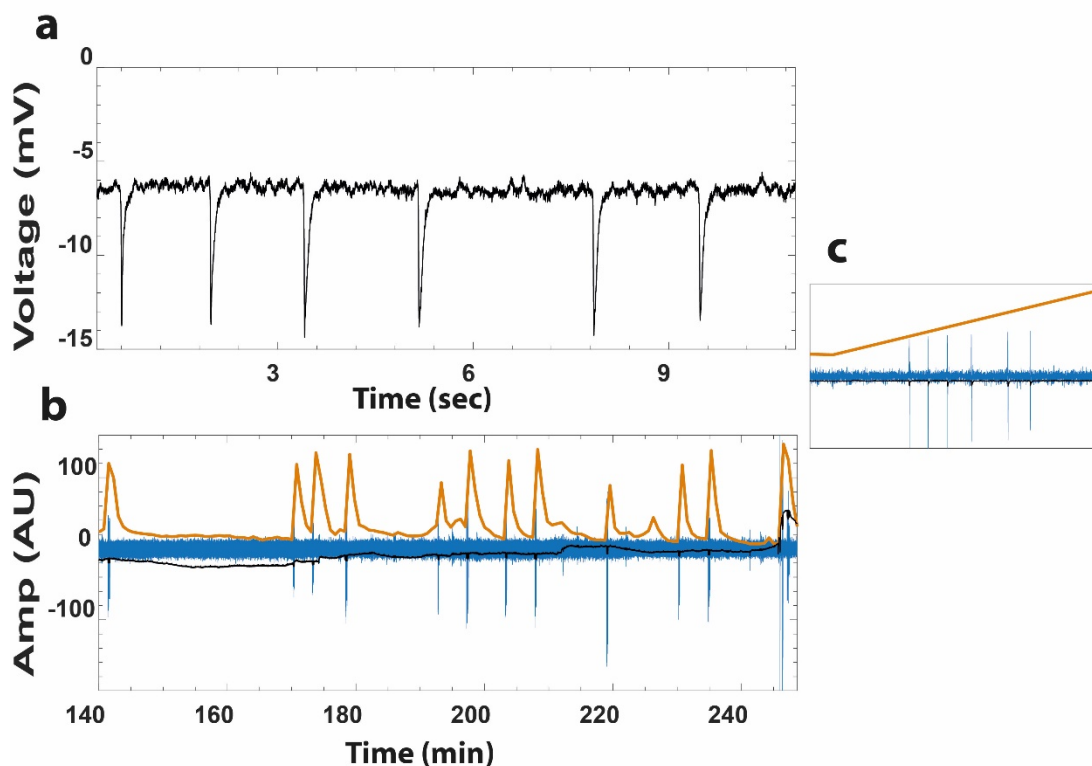




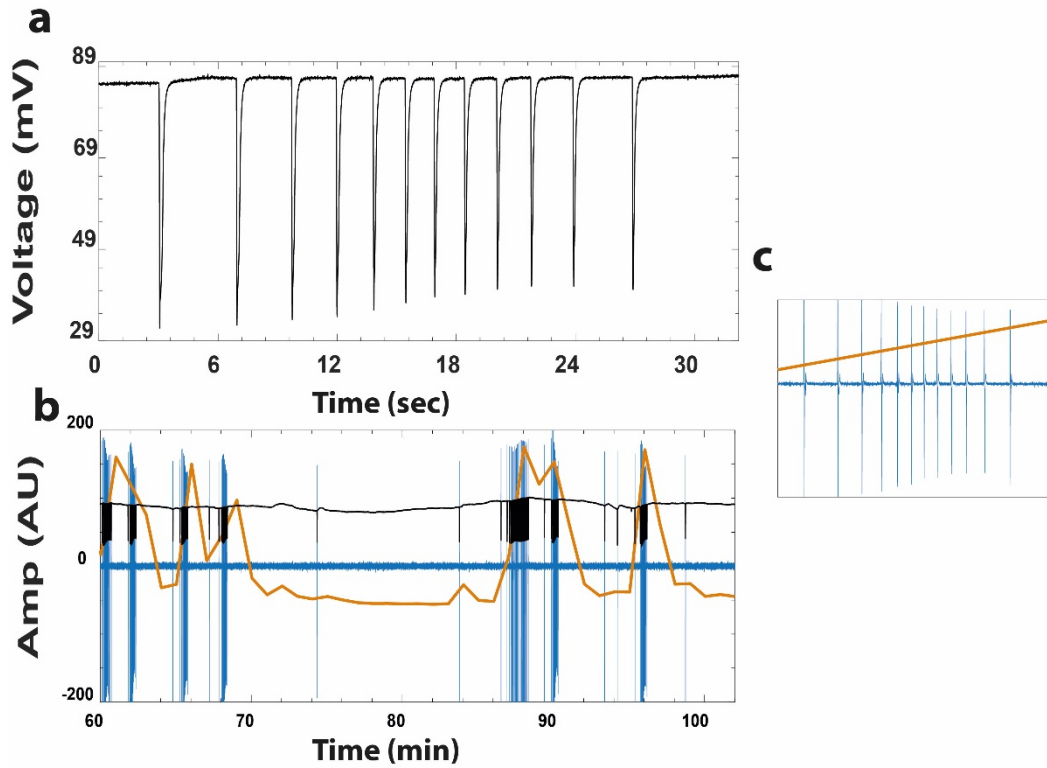
**Extended Data Fig. 5: Frequency threshold.**  $\text{Ca}^{2+}$  activity measured by the fluorescence density as in Fig. 4a in the main text, for two different frequencies of the external electric field. The measurement starts 3 hrs after the tissue excision at  $V=0$  (a) and continues at high voltage (20-26.5 V) at 1 kHz (b), showing enhanced  $\text{Ca}^{2+}$  activity. Switching the frequency of the external AC field to 3 kHz, while maintaining the voltage amplitude at 26.5 V, shows reduction in  $\text{Ca}^{2+}$  activity (c). The images at the right show microscopy images of the sample at the end point of each trace (from left: bright field, low and high  $\text{Ca}^{2+}$  activity depicted by the fluorescence images). They show that the tissue fully regenerates for  $V=0$  and then folds back into a spheroid morphology at high voltage, while resumption of a fully regenerated *Hydra* is observed upon the switch of the frequency to 3 kHz. Bars 100  $\mu\text{m}$  scale.



**Extended Data Fig. 6: Stimulation by elevated potassium.** The trace shows enhanced  $\text{Ca}^{2+}$  activity measured by fluorescence density upon the increase of the potassium ( $\text{K}^+$ ) in the medium from 0.1 mM (normal Hydra medium) to 1 mM at the time marked by the arrow. The measurement starts 3 hrs after the tissue excision. Microscopy images of the sample at the indicated time points (hrs from the excision point) and  $\text{K}^+$  concentrations are shown above the trace in pairs (left: bright field; right  $\text{Ca}^{2+}$  activity depicted by the fluorescence images). The images show that after 61 hrs there are no signs of regeneration in 1 mM  $\text{K}^+$  while all samples at the normal *Hydra* medium (0.1 mM  $\text{K}^+$ ) regenerate within 55 hrs.



**Extended Data Fig. 7a: Electrical measurement in a tissue fragment.** (a) Voltage measurement of a spike burst by a silver-chloride electrode inserted into a tissue fragment embedded in a low-melting 2% agarose gel. (b) Simultaneous recording of  $\text{Ca}^{2+}$  activity by fluorescence microscopy (yellow) and the voltage by an electrode (black). The blue trace shows the voltage spikes extracted from the original voltage measurement by subtracting a smoothed trace (0.1 sec window) from the original one and amplifying the resulting trace (distorting the uniphase spikes, but allowing easy identification of them). Each  $\text{Ca}^{2+}$  spike follows a burst of electrical spikes. The burst in (a) is a zoom over a burst near 190 min in (b). (c) Zoom over one of the  $\text{Ca}^{2+}$  spike events in (b), showing clearly the burst of electrical spikes.



**Extended Data Fig. 7b: Electrical measurement in a spheroid.** (a) Voltage measurement of a spike burst by a silver-chloride electrode inserted into a tissue spheroid (around 3 hrs after excision and folding in solution) embedded in a low-melting 2% agarose gel. (b) The simultaneously recording of  $\text{Ca}^{2+}$  activity by fluorescence microscopy (yellow) and the voltage by an electrode (black). The blue trace shows the voltage spikes extracted from the original voltage measurement as in Fig. 7a. Each  $\text{Ca}^{2+}$  spike follows a burst of electrical spikes. The burst in (a) is a zoom over a burst near 65 min in (b). (c) Zoom over one of the  $\text{Ca}^{2+}$  spike events in (b), showing clearly the burst of electrical spikes.

## Supplementary Videos:

**Movie 1: Reversal of morphogenesis.** Bright-field microscopy movie of a tissue spheroid regenerating into a mature *Hydra* and then folding back its morphology under an electric field. The reversed tissue regenerates again upon the reduction of the external voltage to zero. A second round of reversal of morphogenesis then follows. Note the differences in the critical voltages required for reversal of morphogenesis for the first and second rounds; the voltage range in the first round is 20-30 V while in the second round is 30-40 V. The scale of the image is  $\sim 1.1$  mm and the running time is from the point of tissue excision.

**Movie 2: Decay of *Wnt3* during reversal of morphogenesis.** The same sample as in Movie 1 is observed under a fluorescence microscope for GFP (left) and RFP (right). The GFP is under the *Wnt3* promoter and the RFP is under the control of the ubiquitous *Hydra* actin promoter and serves as a fluorescence reference. The movie shows the two rounds of reversal of morphogenesis as in Movie 1. The scale of the image is  $\sim 1.1$  mm and the running time is from the point of tissue excision.

**Movie 3: Dynamics of  $\text{Ca}^{2+}$  in reversal of morphogenesis under an electric field.** Fluorescence microscopy time-lapse of a strain expressing the GCaMP6s probe reporting  $\text{Ca}^{2+}$  activity in the epithelial cells. The tissue spheroid regenerates under a voltage below the critical value and then folds back as the voltage is increased. The tissue regenerates again upon switching the voltage to zero. The scale of the image is  $\sim 1.1$  mm and the running time is from the point of tissue excision.

**Movie 4: Frequency threshold of the external field.** Bright-field microscopy of a tissue under an external AC electric field at two different frequencies. At 1 kHz and voltage above criticality, the *Hydra* exhibits reversal of morphogenesis and folds into a spheroid while it regenerates again at 3 kHz under the same voltage. The movie shows two rounds of the backward-forward morphogenesis cycle under the frequency switch. The scale of the image is  $\sim 1.1$  mm and the running time is from the point of tissue excision.